Cell Reports

Report

# Oncogene-Selective Sensitivity to Synchronous Cell Death following Modulation of the Amino Acid Nutrient Cystine

## Graphical Abstract

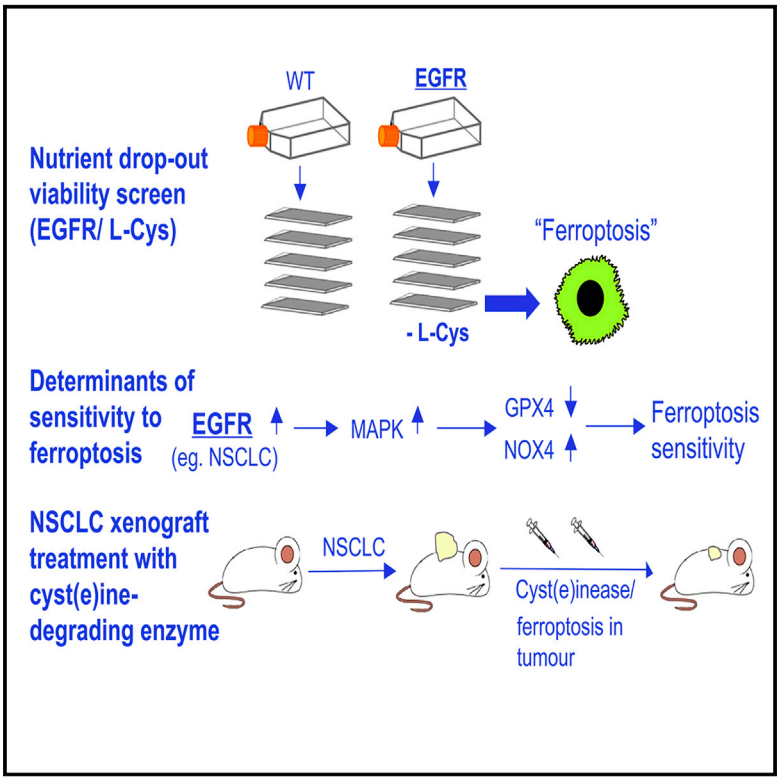


## Highlights

- A nutrient depletion screen revealed a selective role for cystine in promoting viability
- Cystine was shown to promote viability by preventing ferroptosis
- Sensitivity to depletion of cystine was related to activation of MAPK
- Depletion of cystine inhibited tumor growth in a NSCLC xenograft model

## Authors

Ioannis Poursaitidis, Xiaomeng Wang, Thomas Crighton, ..., Scott W. Rowlinson, Everett Stone, Richard F. Lamb

## Correspondence

lambr@hope.ac.uk

## In Brief

Poursaitidis et al. show that EGFR and BRAF mutant cells are sensitive to ferroptosis. Sensitivity was related to activation of MAPK signaling and the generation and release of hydrogen peroxide. To show that this sensitivity can be exploited therapeutically, growth of an EGFR mutant NSCLC xenograft was inhibited by a cyst(e)ine-degrading enzyme.

Poursaitidis et al., 2017, Cell Reports *18*, 2547–2556
March 14, 2017 
http://dx.doi.org/10.1016/j.celrep.2017.02.054

CellPress

Cell Reports
Report



# Oncogene-Selective Sensitivity to Synchronous Cell Death following Modulation of the Amino Acid Nutrient Cystine

Ioannis Poursaitidis,[2,9] Xiaomeng Wang,[2,9] Thomas Crighton,[2] Christiaan Labuschagne,[3] David Mason,[4] Shira L. Cramer,[5] Kendra Triplett,[5] Rajat Roy,[6] Olivier E. Pardo,[6] Michael J. Seckl,[6] Scott W. Rowlinson,[7] Everett Stone,[8] and Richard F. Lamb[1,10,*]

[1]School of Health Sciences, Liverpool Hope University, Hope Park Campus, Liverpool L16 9JD, UK
[2]Department of Molecular and Clinical Cancer Medicine, University of Liverpool North West Cancer Research Centre, University of Liverpool, 200 London Road, Liverpool L69 7ZB, UK
[3]Cancer Research UK Beatson Institute, Switchback Road, Bearsden, Glasgow G61 1BD, UK
[4]Centre for Cell Imaging, Institute of Integrative Biology, University of Liverpool, Biosciences Building, Crown Street, Liverpool L69 7ZB, UK
[5]Department of Chemical Engineering, The University of Texas at Austin, Austin, TX 78712, USA
[6]Division of Cancer CRUK Laboratories, 1st Floor ICTEM Building, Hammersmith Hospital Campus of Imperial College London, Du Cane Road, London W120NN, UK
[7]Aeglea BioTherapeutics, Austin, TX 78746, USA
[8]Department of Molecular Biosciences, The University of Texas at Austin, Austin, TX 78712, USA
[9]Co-first author
[10]Lead Contact
*Correspondence: lambr@hope.ac.uk
http://dx.doi.org/10.1016/j.celrep.2017.02.054

## SUMMARY

**Cancer cells reprogram their metabolism, altering both uptake and utilization of extracellular nutrients. We individually depleted amino acid nutrients from isogenic cells expressing commonly activated oncogenes to identify correspondences between nutrient supply and viability. In HME (human mammary epithelial) cells, deprivation of cystine led to increased cell death in cells expressing an activated epidermal growth factor receptor (EGFR) mutant. Cell death occurred via synchronous ferroptosis, with generation of reactive oxygen species (ROS). Hydrogen peroxide promoted cell death, as both catalase and inhibition of NADPH oxidase 4 (NOX4) blocked ferroptosis. Blockade of EGFR or mitogen-activated protein kinase (MAPK) signaling similarly protected cells from ferroptosis, whereas treatment of xenografts derived from EGFR mutant non-small-cell lung cancer (NSCLC) with a cystine-depleting enzyme inhibited tumor growth in mice. Collectively, our results identify a potentially exploitable sensitization of some EGFR/MAPK-driven tumors to ferroptosis following cystine depletion.**

## INTRODUCTION

Synthetic lethal screens have led to the identification of specific cancer cell vulnerabilities (Barbie et al., 2009; Possik et al., 2014; Scholl et al., 2009). One such vulnerability has previously been exploited therapeutically in acute lymphoblastic leukemia (ALL), where leukemic cells lacking asparagine synthase are known to require the amino acid asparagine and apoptose following administration of asparaginase (Holleman et al., 2003; Tallal et al., 1970). Overall amino acid abundance itself may be higher in cancerous tissue, suggesting an increased need for amino acids in some tumors (Hirayama et al., 2009; Kami et al., 2013). In pancreatic ductal adenocarcinoma (PDAC), KRAS is thought to induce a genetic program that favors metabolism of glutamine, rendering these cells particularly sensitive to glutamine withdrawal (Son et al., 2013). Some tumor cell lines (Scott et al., 2000) and primary tumors (Gonzalez and Byus, 1991) require exogenous arginine, indicating some selectivity in amino acid requirements. Here, we have explored the extracellular amino acid nutrient requirements of cells gene edited to introduce common oncogenic mutations. We identify a selective sensitivity to synchronous cell death by ferroptosis following deprivation of the amino acid nutrient cystine. Sensitization was found to be related to elevated mitogen-activated protein kinase (MAPK) signaling, with synchronous cell death involving hydrogen peroxide generation and release. Finally, we show that enzymatic cystine deprivation in vivo results in an inhibition of tumor growth in an EGFR mutant NSCLC xenograft model, suggesting that, by promoting ferroptosis, cystine depletion provides therapeutic benefit in some tumors.

## RESULTS

### EGFR Mutant HME Cells Undergo Cell Death when Deprived of the Amino Acid Nutrient Cystine

Human mammary epithelial (HME) cells were gene edited to introduce common oncogenic driver mutations (epidermal

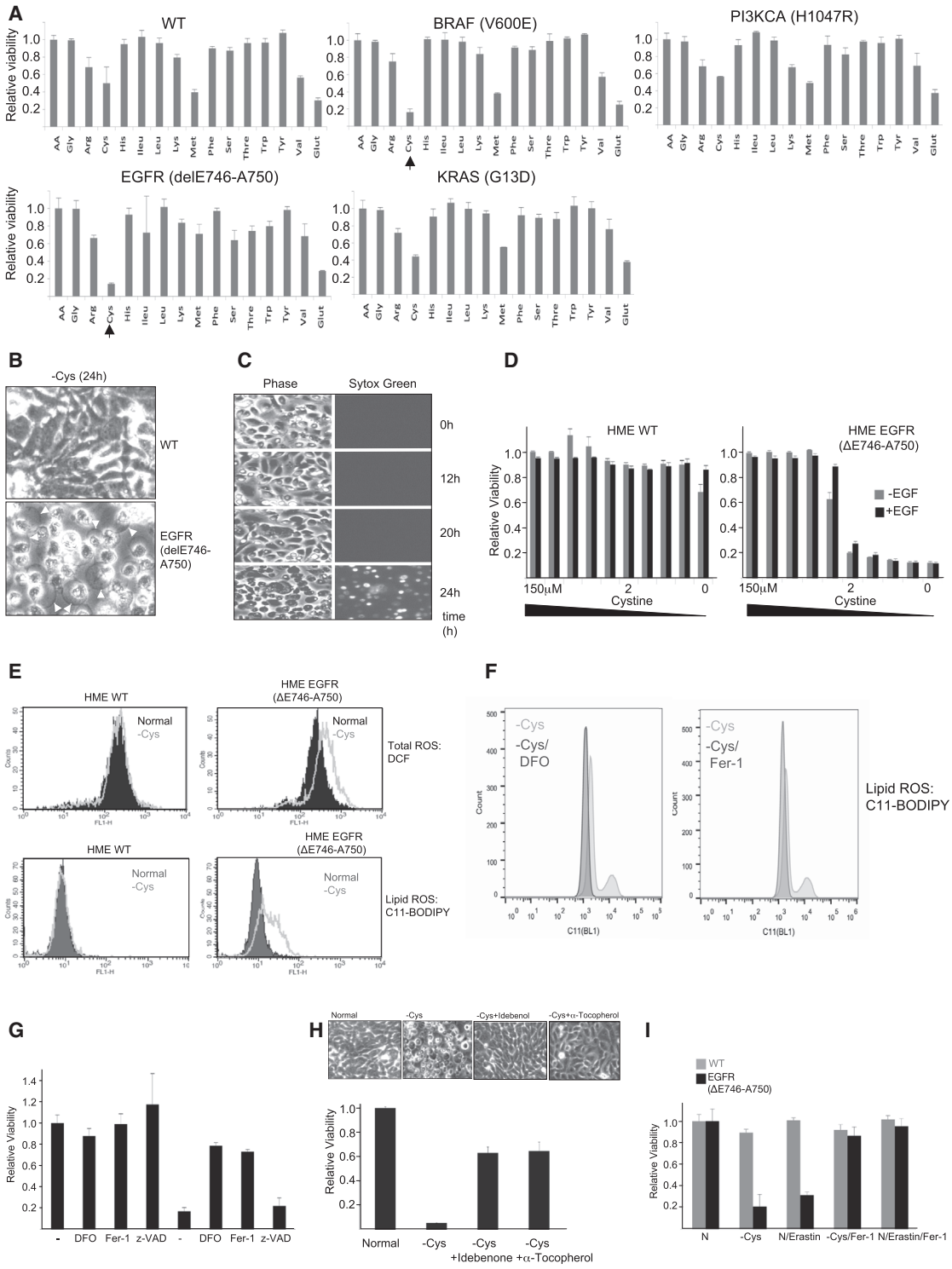


**Figure 1. Deprivation of Cystine Induces Selective Cell Death by Ferroptosis in EGFR Mutant HME Cells**

(A) Cell viability screen of HME cell lines deprived of individual amino acids for 72 hr. Histograms represent the average viability ± SD of three biological replicates relative to complete media assigned a value of 1 (+AA).

(B) Phase contrast micrographs of wild-type (WT) and EGFR (delE746-A750) HME cells deprived of cystine for 24 hr. Arrowheads indicate membrane extrusions.

(C) Time-lapse phase contrast (left) and Sytox Green (right) micrographs of live EGFR (delE746-A750) cells deprived of cystine for various times up to 24 hr.

*(legend continued on next page)*

growth factor receptor [EGFR] [delE746-A750], KRAS [G13D], BRAF [V600E], and PIK3CA [H1047R]) in an otherwise diploid genetic background (Di Nicolantonio et al., 2008). Following culture in media deficient in specific amino acids, we measured cell viability. All lines deprived of L-cystine (cystine) exhibited some loss of viability ranging from 40% to >80%. However, EGFR and BRAF mutant HME cells were especially sensitive, with viability inhibited by >80% (Figure 1A). Cystine deprivation induced a widespread loss of viability in EGFR mutant, but not wild-type HME, cells, with the majority of cells exhibiting a swollen or burst morphology (Figure 1B).

Next, we monitored EGFR mutant HME cells deprived of cystine by video time-lapse microscopy and observed rapid and synchronous cell swelling/bursting (Figure 1C; Movie S1). Sytox Green, a cell-impermeant nuclear stain, synchronously entered cells after cystine depletion (Figure 1C), indicating loss of plasma membrane integrity at <2 μM cystine (Figure 1D). Death was reversible upon re-supplementation of cystine for up to 10 hr but declined progressively thereafter and was not prevented by addition of D-cystine (Figure S1A).

## Cell Death in Cystine-Deprived EGFR Mutant HME Cells Exhibits Hallmarks of Ferroptosis

This type of death resembled ferroptosis, an iron-dependent non-apoptotic cell death (Dixon et al., 2012). Because lipid reactive oxygen species (ROS) accumulation characterizes ferroptosis (Dixon et al., 2012), we measured ROS. Fluorescence-activated cell sorting (FACS) analysis indicated increased ROS accumulation in EGFR mutant HME cells following cystine deprivation (Figure 1E). EGFR mutant HME cells treated with known ferroptosis inhibitors inhibited lipid ROS generation (Figure 1F) and protected EGFR mutant (and BRAF mutant; Figure S1B) cells from cell death (Figure 1G), as did treatment with two other antioxidants (Figure 1H). Finally, erastin, an inhibitor of the system $x_c$-cystine/glutamate antiporter (Dixon et al., 2012), also induced selective loss of viability in EGFR mutant cells (Figure 1H). Collectively, these data indicate that cell death in EGFR mutant cells occurs by ferroptosis.

## MAPK Signaling Sensitizes EGFR Mutant Cells to Cell Death following Cystine Deprivation

EGFR activation results in activation of downstream signaling cascades (Pines et al., 2010). Ferroptosis had previously been shown to require MAPK signaling (Yagoda et al., 2007; Dixon et al., 2012). Treatment of EGFR mutant cells for >24 hr with EGFR or MAPK (MEK and ERK1/2) inhibitors inhibited EGFR and MAPK signaling (Figures 2A and S2A), restored normal adherens junction formation and gap junctional intercellular communication (GJIC) (Figures 2B and 2C), and rescued cell viability following cystine withdrawal (Figures 2D and S2B). Likewise, EGFR and MAPK inhibition in EGFR mutant cells inhibited ROS generation (Figures 2E, S2C, and S2D).

## Cystine Promotes Viability in EGFR Mutant HME Cells via a Glutathione-Independent Mechanism

HME cells might resist ferroptosis by maintaining intracellular levels either of cystine or glutathione, the major cystine-derived antioxidant. To address the former possibility, we deprived cells of cystine and measured activation of GCN2, a sensor of amino acid depletion (Hinnebusch, 2005). However, in both wild-type and EGFR mutant HME cells, GCN2 was equivalently activated following cystine deprivation (Figure 3A). Basal cystine levels were also equivalent and declined similarly in wild-type and EGFR mutant cells following extracellular cystine depletion (Figure S3A). Recent data have suggested a role for glutaminolysis in promoting ferroptosis (Gao et al., 2015). However, both wild-type and EGFR mutant HME cells contained similar steady-state intracellular levels of glutamine that were largely unaltered by deprivation of cystine (Figure S3A). Similarly, total levels of glutathione declined equivalently in wild-type and EGFR mutant HME cells following cystine deprivation (Figure 3B). However, Iressa-treated EGFR mutant cells accumulated more oxidized glutathione (GSSG) in comparison to untreated EGFR mutant HME cells following deprivation of cystine, suggesting that EGFR inhibition increased ROS detoxification (Figure 3C). Surprisingly, an inhibitor of glutathione synthesis (buthionine sulfoximine [BSO]), although also depleting glutathione levels, did not induce cell death (Figure 3D) nor increase ROS in EGFR mutant HME cells, unlike deprivation of cystine (Figure S3B). We therefore asked whether short-term deprivation of cystine, or inhibition of cystine import, acted synergistically with glutathione depletion to induce cell death. Indeed, short-term deprivation of cystine or treatment with inhibitors of the system $x_c$-antiporter induced significantly increased cell death when combined with glutathione depletion (Figure 3E). Treatment with auranofin, an inhibitor of the thioredoxin reductase/thioredoxin (TRX) system (Gromer et al., 1998) implicated in reduction of cystine to cysteine (Mandal et al., 2010; Pader et al., 2014), also synergized with glutathione depletion to promote loss of viability and lipid ROS induction (Figures S3B and S3C). Thus, EGFR mutant cells

(D) Cell viability following titration of cystine in WT and EGFR (delE746-A750) HME cells. Histogram represents the average viability ± SD of cells cultured in various concentrations of cystine ± EGF, relative to complete media (150 μM cystine; assigned an arbitrary value of 1).
(E) ROS in WT HME and EGFR (delE746-A750). (Upper panels) Total ROS measured using CMDCFDA (DCF) is shown; (lower panels) lipid ROS measured using C11 BODIPY 581/591 (C11-BODIPY) is shown. Dark traces, cells cultured in normal media for 12 hr; light traces, cells cultured in media lacking cystine for 12 hr.
(F) Lipid ROS in WT and EGFR (delE746-A750) HME cells. Dark traces, cells cultured in media lacking cystine in the presence of deferoxamine (DFO; 100 μM) or ferrostatin (Fer-1; 2 μM) for 12 hr; light traces, cells cultured in media lacking cystine for 12 hr.
(G) Cell viability of EGFR (delE746-A750) HME cells. Histogram is average viability ± SD cells cultured in normal media (left four bars, untreated [–] assigned an arbitrary value of 1) or media lacking cystine for 24 hr (right four bars) in the presence or absence of DFO, Fer-1, and z-VAD-fMK.
(H) Cell viability (bottom histogram) and phase-contrast microscopy (upper panels) of EGFR (delE746-A750) HME cells. Histogram is average viability ± SD of three biological replicates cultured in normal media (assigned an arbitrary value of 1) or media lacking cystine for 24 hr in the presence or absence of ROS scavengers idebenone and α-tocopherol.
(I) Cell viability of WT (gray bars) and EGFR (delE746-A750; black bars) HME cells. Histogram represents the average viability ± SD cells cultured in normal media or media lacking cystine for 24 hr in the presence or absence of erastin and Fer-1.

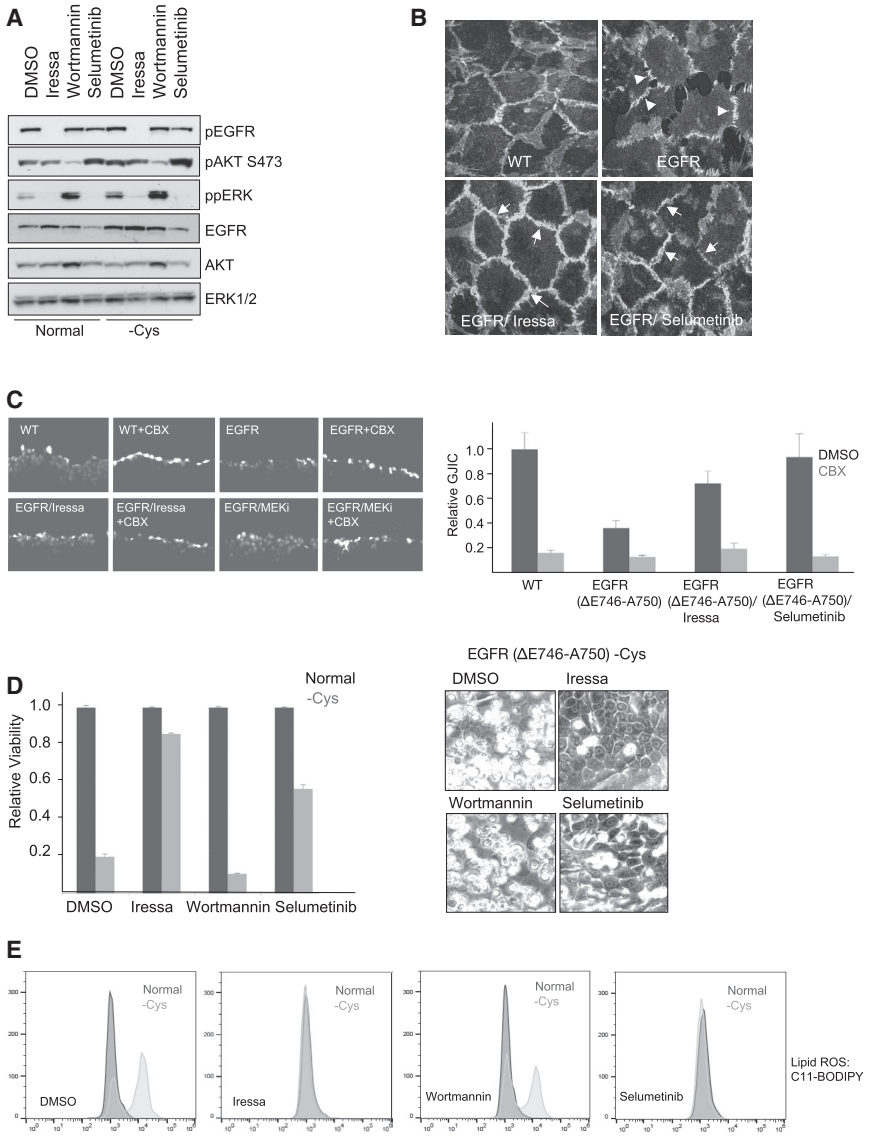


**Figure 2. Active MAPK Signaling Promotes Sensitivity to Cystine Deprivation**

(A) Immunoblots of EGFR (delE746-A750) HME cell lysates probed to detect phosphorylated EGFR, ERK, and AKT from cells cultured in normal media (normal) or media lacking cystine for 12 hr (−Cys) in the presence or absence of inhibitors added for a total of 30 hr.

(B) Confocal micrographs of adherens junctions stained with β-catenin antibody of WT or EGFR (delE746-A750) HME cells treated with vehicle (EGFR) or following treatment with inhibitors for 30 hr. Arrows indicate linear staining for β-catenin at intercellular junctions; arrowheads indicate presence of discontinuous adherens junctions.

(C) (Left panels) Fluorescence micrographs of GJIC measured by lucifer yellow infiltration in WT, EGFR (delE746-A750), Iressa-treated EGFR (delE746-A750; EGFR/Iressa), and selumetinib-treated EGFR (delE746-A750; EGFR/MEKi) in the presence or absence of carbenoxolone (CBX). (Right histogram) Quantification of GJIC is shown. Each condition was analyzed in six random 20× fields in three biological replicates with the values shown representing the mean and SEM and expressed relative to GJIC in WT HME cells assigned an arbitrary value of 1. Light bars represent GJIC in the presence of CBX.

(D) Cell viability (left histogram) and phase-contrast micrographs (right panels) of EGFR (delE746-A750) HME cells treated with inhibitors. Histogram is viability ± SD of cells cultured in normal media (dark bars) or media lacking cystine for 16 hr (light bars) in the presence or absence of inhibitors. Results were expressed for each condition separately, with viability in normal media assigned the arbitrary value of 1.

(E) FACS analyses of lipid ROS in EGFR (delE746-A750) cells following treatment with inhibitors. Dark traces, cells cultured in normal media; light traces, cells cultured in media lacking cystine for 12 hr.

oxidize less glutathione during cystine deprivation, contributing to ROS accumulation, whereas intracellular cysteine appears to play an additional role, aside from glutathione synthesis, in counteracting ROS and ferroptosis.

## GPX4 Is Downregulated in EGFR Mutant HME Cells via MAPK Signaling and Modulates Sensitivity to Cell Death upon Cystine Deprivation

Glutathione peroxidases (GPXs) are good candidates for mediating sensitivity to ferroptosis. GPX4 has previously been implicated in ferroptosis (Friedmann Angeli et al., 2014; Yang et al., 2014), whereas GPX4 is induced following treatment with a BRAF inhibitor (Parmenter et al., 2014). By immunoblotting, GPX4, but not GPX1, expression was upregulated following either EGFR or MAPK (MEK and ERK; Figure S3D) inhibition, whereas GPX2 was not expressed in these cells (Figure 3E) and GPX3 is a secreted GPX expressed in the kidney (Maser et al., 1994). Suppression of GPX4 strongly promoted cell death in both wild-type (Figure 3G) and Iressa-treated EGFR mutant cells (Figure 3H). Lipid ROS similarly increased after suppression of GPX4 (Figure 3I). Thus, downregulation of GPX4 in EGFR mutant HME cells conferred increased sensitivity to ferroptosis following cystine deprivation. To determine whether loss of viability was related to low levels of GPX4, we expressed Flag-GPX4 in EGFR mutant cells. Indeed, ectopic expression of GPX4 significantly increased viability following deprivation of cystine (Figure 3J). Thus, downregulation of GPX4 plays a key role in sensitizing EGFR mutant HME cells to ferroptosis.

## Synchronous Cell Death in EGFR Mutant HME Cells Involves Generation and Release of Hydrogen Peroxide

Hydrogen peroxide is implicated in synchronous ferroptosis in kidney tubule epithelia (Linkermann et al., 2014). Media

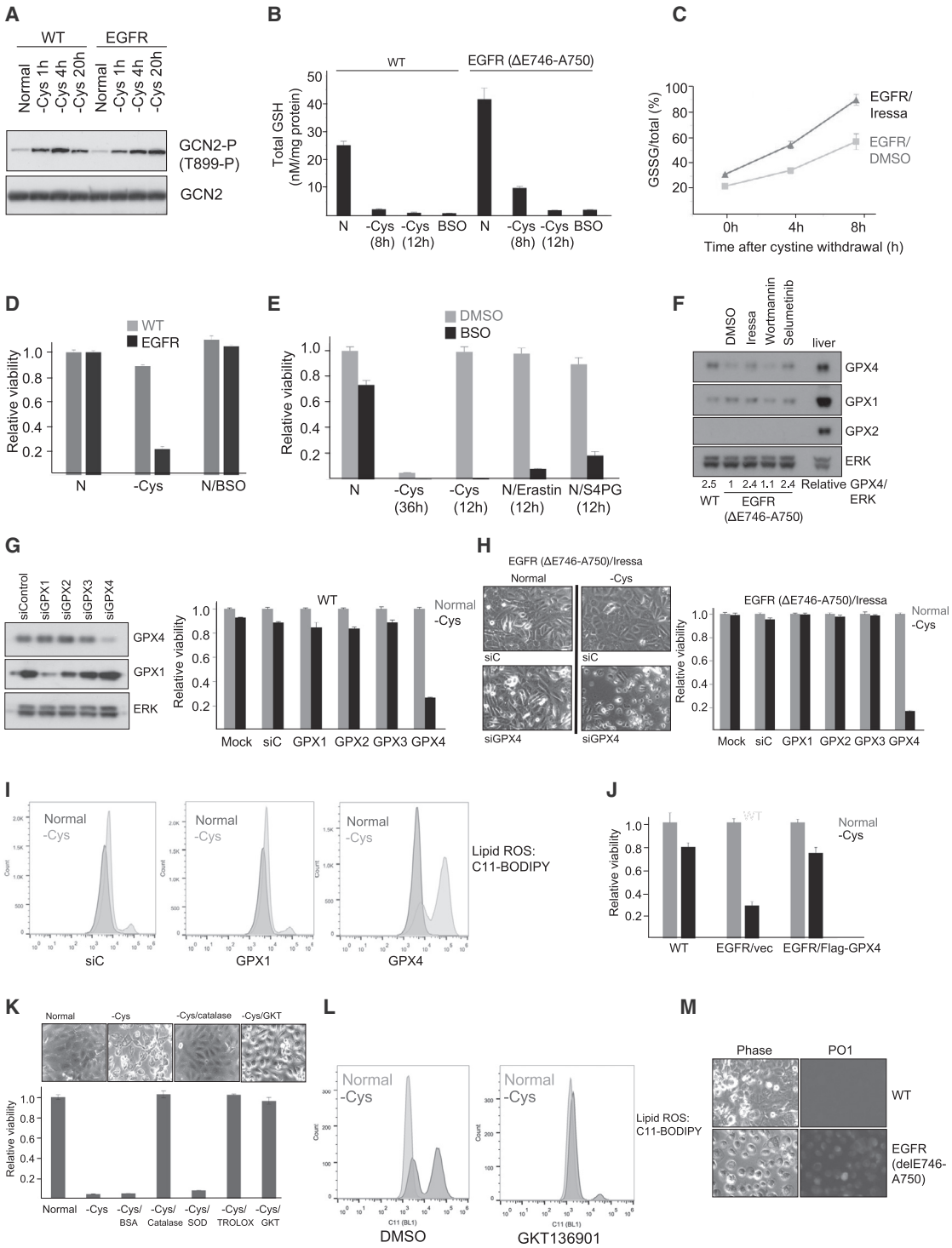


**Figure 3. Involvement of Intracellular Cysteine, GPX4, and Hydrogen Peroxide in Sensitivity to Ferroptosis**

(A) Immunoblots of cell lysates probed with an antibody to active GCN2 (T899-P). Cells were cultured in normal media for 24 hr (normal) or media lacking cystine for various times.

(B) Histogram of total glutathione levels in WT and EGFR (delE746-A750) cells cultured in normal media for 12 hr (N) or media lacking cystine for 8 or 12 hr. As a positive control, BSO was added to cells for 12 hr to deplete the glutathione pool by inhibiting glutathione synthesis.

(C) Time course of glutathione oxidation (GSSG/total) in EGFR (delE746-A750) treated with vehicle (EGFR/DMSO) or Iressa for 30 hr (EGFR/Iressa). Cells were cultured in media lacking cystine for 4 or 8 hr. Chart displays the average ratio of oxidized glutathione (GSSG) to total glutathione (GSH+GSSG) of three biological replicates.

*(legend continued on next page)*

containing soluble catalase similarly rescued viability of EGFR mutant HME cells (Figure 3K). Hydrogen peroxide is produced by NADPH oxidase 4 (NOX4) (Takac et al., 2011). A NOX4 inhibitor (GKT136901; Laleu et al., 2010) also rescued viability, to the same degree as addition of catalase (Figure 3K), and inhibited lipid ROS generation (Figure 3L). NOX4 expression was also increased in EGFR mutant HME cells and downregulated by both EGFR and MAPK inhibition (Figure S3E). Finally, increased accumulation of hydrogen peroxide was detected following deprivation of cystine in EGFR mutant cells (Dickinson et al., 2010; Figure 3M). Thus, hydrogen peroxide contributes to loss of viability of EGFR mutant HME cells deprived of cystine.

### NSCLC Tumor Cell Lines Exhibit a Targetable Sensitivity to Ferroptosis

Mutations in the EGF receptor are found in non-small-cell lung cancers (NSCLCs) (Pao et al., 2004) that are sensitive to tyrosine kinase inhibitors (TKIs) (Paez et al., 2004). We removed cystine from NSCLC cell lines and measured viability and MAPK activation. Of nine NSCLC cell lines tested, three with the highest MAPK signaling (Figure S4A) demonstrated significant loss of viability following withdrawal of cystine (Figures 4A and S4B). In H3255 cells (EGFR L858R mutant), sensitivity was reversed by either EGFR or MAPK inhibition, whereas in Calu-6 cells (KRAS Q61K mutant), sensitivity was reversed by MAPK, but not EGFR, inhibition (Figure S4C). Thus, in NSCLC cell lines, the magnitude of MAPK activation is an important determinant in sensitization to ferroptosis, rather than the nature of the specific oncogenic driver that promotes MAPK signaling. In NCI-NH1650 cells (EGFR delE746-A750), viability was restored by addition of either $\alpha$-tocopherol, the ferroptosis inhibitor Fer-1 (Figure 4B), or Iressa (data not shown) following cystine depletion, indicating that ferroptosis and EGFR signaling were responsible for loss of viability. Surprisingly, however, MEK inhibition in these cells did not rescue viability following cystine depletion (data not shown). Thus, MAPK activation may not invariably promote sensitivity to ferroptosis, and other unknown EGFR-dependent signaling pathway(s) can substitute.

Survival after treatment with TKIs in NSCLC is typically less than 1 year, with patients developing secondary EGFR mutations (Stewart et al., 2015). We therefore sought to determine whether EGFR mutant NSCLC cells might be responsive to low levels of cystine, potentially offering additional therapeutic options utilizing a novel cystine/cysteine-degrading enzyme (cyst(e)inase; AECase) engineered from cystathionine-$\gamma$-lyase (Cramer et al., 2017). Addition of AECase reduced viability in both HME delE746-A750 EGFR or NCI-NH1650 cells (Figures 4C and 4D) and induced widespread uptake of Sytox Green (Figure 4D; Movie S2). Finally, we injected mice bearing established NCI-NH1650 xenografts with AECase. Mirroring the in vitro results, tumor growth was significantly retarded in AECase-treated groups ($p = 0.0001$; Figure 4E). AECase-treated mice were also found to upregulate expression of COX2 (Figure 4F), indicating that they had experienced cystine depletion and initiated ferroptosis within the tumor (Yang et al., 2014). Thus, inhibition of tumor growth can be achieved in tumors sensitive to ferroptosis by enzymatic degradation of cystine/cysteine in vivo.

## DISCUSSION

Cell death by ferroptosis has been implicated in diverse processes (Yang and Stockwell, 2016). Previous data indicated that ferroptosis could be induced preferentially in cells overexpressing mutant RAS oncoproteins (Dixon et al., 2012; Dolma et al., 2003; Yang and Stockwell, 2008) and in some sensitive cell lines could be blocked by MAPK inhibition (Yagoda et al., 2007).

(D) Cell viability of WT (light bars) or EGFR (delE746-A750; dark bars) HME cells. Histogram represents the average viability ± SD of cells cultured for 24 hr in normal media (N), normal media containing 200 μM BSO (N/BSO), or media lacking cystine (−Cys).

(E) Cell viability of EGFR (delE746-A750) pre-treated for 18 hr with DMSO vehicle (light bars) or 200 μM BSO (dark bars) in normal media (N), in normal media containing erastin (N/Erastin), or S4PG (N/S4PG) for 12 hr or following removal of cystine for 36 or 12 hr. Histogram represents the average viability ± SD of cells cultured in normal media (assigned a value of 1).

(F) Immunoblots of WT and EGFR (delE746-A750) cell lysates probed for GPX4, GPX1, GPX2, and ERK in the presence or absence of inhibitors. Relative GPX4/ERK was calculated using ImageJ from scanned autoradiographs of three biological replicates, with the ratio in EGFR (delE746-A750) cells assigned a value of 1.

(G) (Left panels) Immunoblots of WT HME lysates probed for GPX4, GPX1, and ERK1/2. (Right) Histogram of cell viability of HME cells cultured in normal media (light bars) or media lacking cystine (dark bars) for 24 hr. Histogram represents the average viability ± SD following knockdown GPX1–4. Results were expressed for each condition separately, with viability in normal media assigned a value of 1.

(H) (Left panels) Phase-contrast micrographs of EGFR (delE746-A750) HME cells following transfection with control (siC) or GPX4 small interfering RNAs (siRNAs) (siGPX4) and treated with Iressa for 30 hr followed by culture in normal media or media lacking cystine for 24 hr. (Right) Histogram is viability ± SD after knockdown of GPX1–4 in Iressa-treated EGFR (delE746-A750) cells. Viability of cells cultured in normal media (light bars) or media lacking cystine (dark bars) were determined. Results were expressed for each condition separately, with viability in normal media assigned the arbitrary value of 1.

(I) FACS analyses of lipid ROS in WT HME cells following knockdown of GPX1 and GPX4. Dark traces, cells cultured in normal media; light traces, cells cultured in media lacking cystine for 12 hr.

(J) Histogram is shown representing the average viability ± SD following overexpression of Flag-GPX4 (Mannes et al., 2011) in EGFR (delE746-A750) cells. Viability of WT HME cells or vector- or GPX4-transfected EGFR (delE746-A750) cells cultured in normal media (light bars) or media lacking cystine (dark bars) for 16 hr is shown. Results were expressed for each condition separately, with viability in normal media assigned a value of 1.

(K) (Top panels) Phase-contrast micrographs of EGFR (delE746-A750) HME cells in normal media or media deprived of cystine alone or containing catalase or GKT136901. (Bottom) Histogram representing the average viability ± SD of EGFR (delE746-A750) HME cells cultured for 24 hr in normal media (normal; assigned a value of 1) or media lacking cystine alone (−Cys) or with BSA, catalase, superoxide dismutase (SOD), Trolox, or GKT136901 added is shown.

(L) FACS analyses of lipid ROS in EGFR (delE746-A750) HME cells following treatment with the NOX4 inhibitor GKT136901. Dark traces, cells cultured in media lacking cystine; light traces, cells cultured in normal media.

(M) Live images of hydrogen peroxide detected with PO1. (Left) Phase-contrast images of WT and EGFR (delE746-A750) cells deprived of cystine for 24 hr and incubated with PO1 (right panels) are shown.

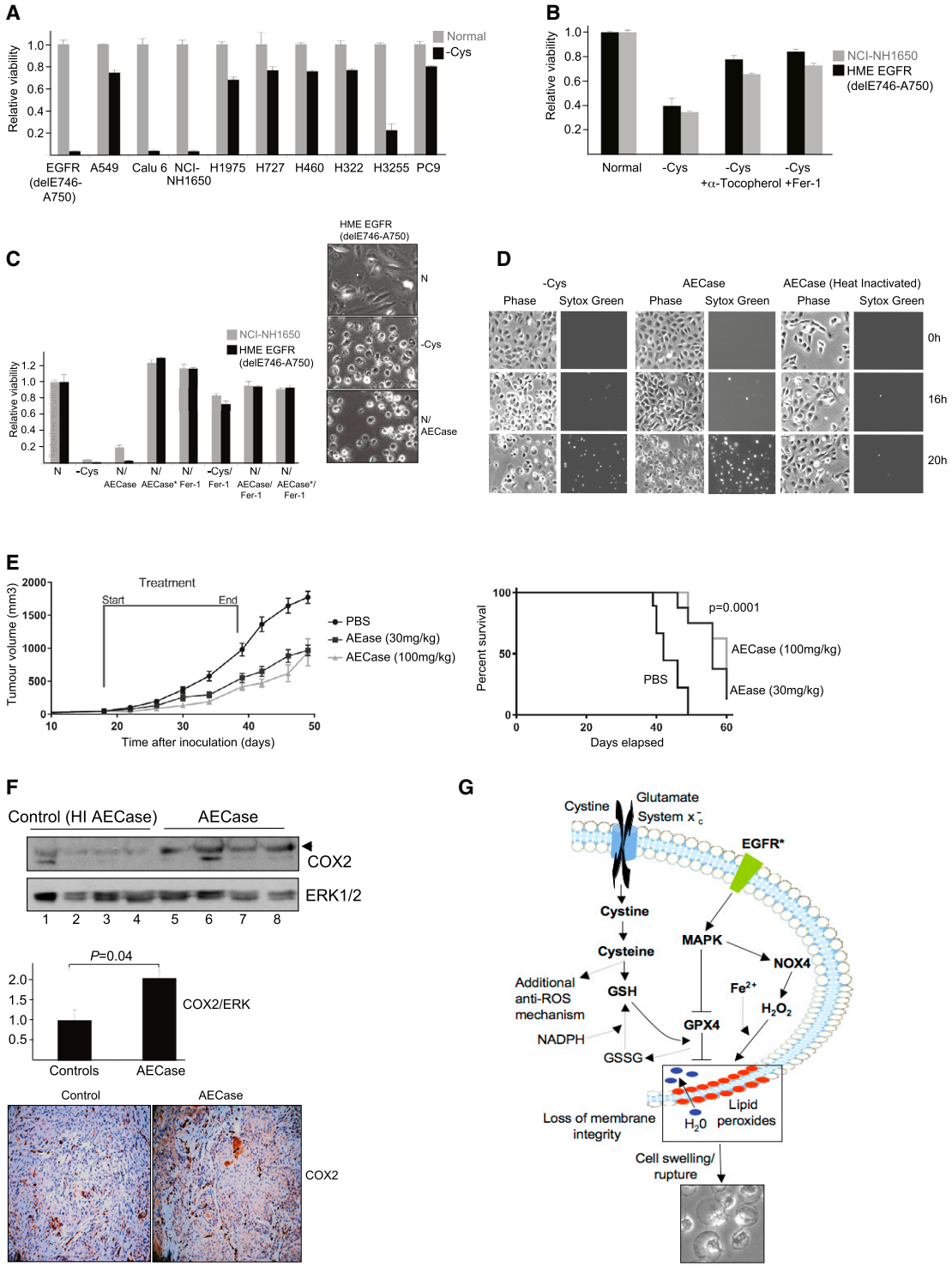


**Figure 4. Ferroptosis Is Induced in Some NSCLC Cell Lines and Inhibits Tumor Growth**

(A) Histogram of viability ± SD of EGFR (delE746-A750) HME and NSCLC cell lines cultured for 72 hr in normal media (light bars) or media lacking cystine (dark bars). Results were expressed for each cell line separately, with viability in normal media assigned a value of 1.

(B) Histogram representing the average viability ± SD of EGFR (delE746-A750) HME (dark bars) or NCI-NH1650 (light bars) cultured for 72 hr in normal media (N), normal media containing ferrostatin (N/Fer-1), media lacking cystine (−Cys), or media lacking cystine in the presence of α-tocopherol or Fer-1. Results were expressed for each cell line separately, with viability in normal media assigned a value of 1.

*(legend continued on next page)*

We identify here a selective cell death of EGFR mutant cells deprived of the amino acid cystine. Death was associated with synchronous loss of plasma membrane integrity. By a variety of criteria, this mode of cell death is ferroptosis. In our model (Figure 4G), active MAPK signaling downstream of active EGFR can sensitize cells to ferroptosis upon cystine depletion. Sensitization involves both impaired detoxification of lipid peroxides, due to reduced expression of GPX4, and generation of hydrogen peroxide, via NOX4. A major consequence of lipid peroxidation is loss of impermeability to water (Lis et al., 2011; Wong-Ekkabut et al., 2007), providing an explanation for the characteristic cell swelling and rupture we observe.

Sensitivity to induction of ferroptosis or cystine deprivation is likely to be modulated by additional, and possibly MAPK-independent, mechanisms, such as the utilization of the sulfur-containing amino acid methionine via the transsulfuration pathway (Hayano et al., 2016). Our results suggest, however, the possibility of exploiting ferroptosis sensitivity in a translational manner. Tumors with sustained MAPK activation, as found in NSCLC, are likely to respond to cystine depletion in vivo by inducing ferroptosis. Our results indicate that an enzymatic approach (Cramer et al., 2017) may be effective in reducing cystine levels in vivo, inducing ferroptosis. Collectively, our work indicates that it might therefore be possible both to identify tumors exhibiting increased sensitivity to ferroptosis and to treat them via cycles of cystine depletion.

## EXPERIMENTAL PROCEDURES

### Cell Culture and Treatments

The hTERT-HME cell lines were a kind gift from Prof. Alberto Bardelli (Institute for Cancer Research and Treatment, IRCC). Cells were grown in DMEM media as described (Di Nicolantonio et al., 2008). To deprive individual amino acids, cells were washed once in DMEM media lacking all amino acids (−AA) and switched to specific amino-acid-free media. DMEM media used for deprivation were made from powdered AA-free DMEM (US Biological), with 10% dialyzed fetal bovine serum (FBS) and additives (Di Nicolantonio et al., 2008). Amino acids (Sigma) at 50× concentrations in water were added at 1× concentration. All amino acids were added for complete media (+AA), with individual DMEM amino acids omitted to generate single amino-acid-deficient media. For the initial screen, 30,000 cells were plated per well in a 96-well plate and switched after 24 hr to depleted amino acid media for 72 hr. Viability was assessed in the initial screen using Calcein AM (Molecular Probes; ThermoFisher) at 1 μM for 2 hr and cells fixed for 15 min with 4% paraformaldehyde prior to analysis on a Genios plate reader and in all other experiments using the CellTiter-Glo luminescence assay (Promega).

### FACS Analysis

To detect ROS, 200,000 cells were plated in 6-well plates and switched to cystine-deprived media for 12 hr prior to FACS analysis. CMDCFDA and C11-BODIPY581/591 (Molecular Probes; Thermo Fisher) were used to detect total and lipid ROS, respectively. Following deprivation of cystine for 12 hr, cells were washed with PBS, loaded with either CMDCFDA (10 μM) or C11 BODIPY (2 μM) in DPBS for 30 min, trypsinized with 0.25% Trypsin-EDTA, resuspended in PBS with 1% FBS, and analyzed using an Attune NxT flow cytometer (Thermo Fisher). Dyes were excited using a blue 488-nm laser, and emission was recorded on BL1 (530/30) for a minimum of 5,000 cells per sample.

### Xenograft Tumor Model

2.5× 105 NCI-H1650 cells were inoculated 1:1 in Matrigel: PBS (100 mL) by subcutaneous injection into eight non-obese diabetic (NOD) severe combined immunodeficiency (SCID) gamma male mice. Tumors were allowed to engraft and grow for 30 days (tumor volume averaged ~200 mm3) and mice treated by intraperitoneal (i.p.) injection with 100 mg/kg cyst(e)inase or 100 mg/kg heat-inactivated cyst(e)inase (n = 4 ea.) on day 30, with a second dose given on day 33. Mice were necropsied 24 hr after the second dose. For analyses of COX2, control and treated tumors were excised and one-half preserved in 10% neutral buffered formalin for immunohistochemistry (IHC) and the remaining half frozen in liquid nitrogen for protein extraction. For IHC, anti-COX2 from Abcam (ab15191) was used with DAB detection.

### Statistical Analyses

Data were analyzed using Microsoft Excel or GraphPad Prism software (GraphPad) and are presented as mean values ± SEM. All viability data represent the mean of three biological replicates/condition. Statistical analyses were performed using two-sided Student's t test. For Kaplan-Meier plots, statistical significance was analyzed by the log rank (Mantel-Cox) test. Sample variance was not significant between control and treatment groups prior to study onset. Significance was set at $p < 0.05$. All data are representative of at least two independent experiments.

## SUPPLEMENTAL INFORMATION

Supplemental Information includes Supplemental Experimental Procedures, four figures, and two movies and can be found with this article online at http://dx.doi.org/10.1016/j.celrep.2017.02.054.

(C) (Left) Histogram of viability ± SD of EGFR (delE746-A750) HME (dark bars) or NCI-NH1650 (light bars) cells cultured for 48 hr in normal media (N) (assigned a value of 1), media lacking cystine (−Cys), normal media containing 125 nM cyst(e)inase (AECase) on its own (N/AECase) or with Fer-1 (N/AECase/Fer-1), or normal media containing 125 nM heat-inactivated AECase on its own (N/AECase*) or with Fer-1 (N/AECase*/Fer-1). (Right) Phase-contrast micrographs of EGFR (delE746-A750) HME cells in normal media, media deprived of cysteine, or normal media containing 125 nM AECase (N/AECase) for 48 hr are shown.

(D) Phase contrast (left), and Sytox Green (right) micrographs of H1650 cells deprived of cystine (left panels), treated with 125 nM AECase (middle panels), or treated with heat-inactivated AECase (right panels) for various times up to 20 hr.

(E) Cyst(e)inase (AECase) administration inhibits tumor growth in a NCI-NH1650 xenograft mouse model. (Left panel) Increase in tumor volume following i.p. administration of PBS control (dark circles) or 30 mg/kg (dark squares) or 100 mg/kg (light triangles) AECase is shown. Start and end of treatment times are also shown. (Right panel) Kaplan-Meier plots of median survival of PBS- or AECase-treated tumor-bearing mice are shown.

(F) (Top panels) Immunoblots of lysates from control (lanes 1–4) or AECase-treated (lanes 5–8) NCI-NH1650 xenograft lysates probed to detect COX2 (arrowhead). (Middle histogram) Quantification of relative COX2/ERK in control or AECase-treated groups is shown. $p = 0.04$; $n = 4$. (Bottom micrographs) Images of COX2 staining in control and AECase-treated tumors are shown.

(G) Model depicting role of activated EGFR in determining sensitivity to ferroptosis. Activated EGFR (EGFR*) stimulates MAPK signaling, reducing expression of GPX4 and inducing expression of NOX4. GPX4 utilizes reduced glutathione (GSH) derived from cystine transported via the System $x_c^-$ cystine-glutamate exchanger to detoxify membrane lipid peroxides (red), generating oxidized glutathione (GSSG). GSSG is recycled to GSH using reducing equivalents derived from NADPH (dashed line). Cystine can be reduced to generate cysteine that can independently detoxify ROS and may have additional functions (e.g., Briggs et al., 2016). Lipid peroxides are generated from hydrogen peroxide ($H_2O_2$, derived from NOX4) and iron ($Fe^{2+}$), producing hydroxyl radicals that initiate lipid peroxidation. Lipid peroxidation leads to loss of membrane integrity, allowing uptake of water, cell swelling, and rupture.

## AUTHOR CONTRIBUTIONS

I.P. and X.W. performed cell viability assays, inhibitor and siRNA treatments, FACS analyses, and immunoblotting experiments; T.C. performed immunofluorescence and assays of GJIC; C.L. performed amino acid analyses; D.M. assisted with methods of quantification; S.L.C., K.T., and E.S. designed and performed the xenograft experiments; R.R., O.E.P., and M.J.S. provided NSCLC cell lines; and S.W.R. provided AECase. R.F.L. conceived the study and wrote the paper.

## ACKNOWLEDGMENTS

The p442-PL1 Flag-Strep-HA-GPx4 (Flag-GPX4) was from Marcus Konrad. We are grateful for the support of John Neoptolemos and to Cancer Research UK and the Liverpool Pancreatic Biomedical Research Unit for funding (to I.P. and R.F.L.). R.R. was supported by the Cancer Treatment and Research Trust and M.J.S. by the Imperial National Institute for Health Research (NIHR) Biomedical Research Centre and Imperial CRUK/NIHR Experimental Cancer Medicine Centre. X.W. and R.F.L. acknowledge support from North West Cancer Research and D.M. from the Medical Research Council. E.S. is an inventor on intellectual property related to part of this work, and E.S. and S.W.R. have an equity interest in Aeglea Biotherapeutics.

Received: August 8, 2016
Revised: November 30, 2016
Accepted: February 16, 2017
Published: March 14, 2017

## REFERENCES

Barbie, D.A., Tamayo, P., Boehm, J.S., Kim, S.Y., Moody, S.E., Dunn, I.F., Schinzel, A.C., Sandy, P., Meylan, E., Scholl, C., et al. (2009). Systematic RNA interference reveals that oncogenic KRAS-driven cancers require TBK1. Nature *462*, 108–112.

Briggs, K.J., Koivunen, P., Cao, S., Backus, K.M., Olenchock, B.A., Patel, H., Zhang, Q., Signoretti, S., Gerfen, G.J., Richardson, A.L., et al. (2016). Paracrine Induction of HIF by Glutamate in Breast Cancer: EglN1 Senses Cysteine. Cell *166*, 126–139.

Cramer, S.L., Saha, A., Liu, J., Tadi, S., Tiziani, S., Yan, W., Triplett, K., Lamb, C., Alters, S.E., Rowlinson, S., et al. (2017). Systemic depletion of L-cyst(e)ine with cyst(e)inase increases reactive oxygen species and suppresses tumor growth. Nat. Med. *23*, 120–127.

Di Nicolantonio, F., Arena, S., Gallicchio, M., Zecchin, D., Martini, M., Flonta, S.E., Stella, G.M., Lamba, S., Cancelliere, C., Russo, M., et al. (2008). Replacement of normal with mutant alleles in the genome of normal human cells unveils mutation-specific drug responses. Proc. Natl. Acad. Sci. USA *105*, 20864–20869.

Dickinson, B.C., Huynh, C., and Chang, C.J. (2010). A palette of fluorescent probes with varying emission colors for imaging hydrogen peroxide signaling in living cells. J. Am. Chem. Soc. *132*, 5906–5915.

Dixon, S.J., Lemberg, K.M., Lamprecht, M.R., Skouta, R., Zaitsev, E.M., Gleason, C.E., Patel, D.N., Bauer, A.J., Cantley, A.M., Yang, W.S., et al. (2012). Ferroptosis: an iron-dependent form of nonapoptotic cell death. Cell *149*, 1060–1072.

Dolma, S., Lessnick, S.L., Hahn, W.C., and Stockwell, B.R. (2003). Identification of genotype-selective antitumor agents using synthetic lethal chemical screening in engineered human tumor cells. Cancer Cell *3*, 285–296.

Friedmann Angeli, J.P., Schneider, M., Proneth, B., Tyurina, Y.Y., Tyurin, V.A., Hammond, V.J., Herbach, N., Aichler, M., Walch, A., Eggenhofer, E., et al. (2014). Inactivation of the ferroptosis regulator Gpx4 triggers acute renal failure in mice. Nat. Cell Biol. *16*, 1180–1191.

Gao, M., Monian, P., Quadri, N., Ramasamy, R., and Jiang, X. (2015). Glutaminolysis and transferrin regulate ferroptosis. Mol. Cell *59*, 298–308.

Gonzalez, G.G., and Byus, C.V. (1991). Effect of dietary arginine restriction upon ornithine and polyamine metabolism during two-stage epidermal carcinogenesis in the mouse. Cancer Res. *51*, 2932–2939.

Gromer, S., Arscott, L.D., Williams, C.H., Jr., Schirmer, R.H., and Becker, K. (1998). Human placenta thioredoxin reductase. Isolation of the selenoenzyme, steady state kinetics, and inhibition by therapeutic gold compounds. J. Biol. Chem. *273*, 20096–20101.

Hayano, M., Yang, W.S., Corn, C.K., Pagano, N.C., and Stockwell, B.R. (2016). Loss of cysteinyl-tRNA synthetase (CARS) induces the transsulfuration pathway and inhibits ferroptosis induced by cystine deprivation. Cell Death Differ. *23*, 270–278.

Hinnebusch, A.G. (2005). Translational regulation of GCN4 and the general amino acid control of yeast. Annu. Rev. Microbiol. *59*, 407–450.

Hirayama, A., Kami, K., Sugimoto, M., Sugawara, M., Toki, N., Onozuka, H., Kinoshita, T., Saito, N., Ochiai, A., Tomita, M., et al. (2009). Quantitative metabolome profiling of colon and stomach cancer microenvironment by capillary electrophoresis time-of-flight mass spectrometry. Cancer Res. *69*, 4918–4925.

Holleman, A., den Boer, M.L., Kazemier, K.M., Janka-Schaub, G.E., and Pieters, R. (2003). Resistance to different classes of drugs is associated with impaired apoptosis in childhood acute lymphoblastic leukemia. Blood *102*, 4541–4546.

Kami, K., Fujimori, T., Sato, H., Sato, M., Yamamoto, H., Ohashi, Y., Sugiyama, N., Ishihama, Y., Onozuka, H., Ochiai, A., et al. (2013). Metabolomic profiling of lung and prostate tumor tissues by capillary electrophoresis time-of-flight mass spectrometry. Metabolomics *9*, 444–453.

Laleu, B., Gaggini, F., Orchard, M., Fioraso-Cartier, L., Cagnon, L., Houngninou-Molango, S., Gradia, A., Duboux, G., Merlot, C., Heitz, F., et al. (2010). First in class, potent, and orally bioavailable NADPH oxidase isoform 4 (Nox4) inhibitors for the treatment of idiopathic pulmonary fibrosis. J. Med. Chem. *53*, 7715–7730.

Linkermann, A., Skouta, R., Himmerkus, N., Mulay, S.R., Dewitz, C., De Zen, F., Prokai, A., Zuchtriegel, G., Krombach, F., Welz, P.S., et al. (2014). Synchronized renal tubular cell death involves ferroptosis. Proc. Natl. Acad. Sci. USA *111*, 16836–16841.

Lis, M., Wizert, A., Przybylo, M., Langner, M., Swiatek, J., Jungwirth, P., and Cwiklik, L. (2011). The effect of lipid oxidation on the water permeability of phospholipids bilayers. Phys. Chem. Chem. Phys. *13*, 17555–17563.

Mandal, P.K., Seiler, A., Perisic, T., Kölle, P., Banjac Canak, A., Förster, H., Weiss, N., Kremmer, E., Lieberman, M.W., Bannai, S., et al. (2010). System x(c)- and thioredoxin reductase 1 cooperatively rescue glutathione deficiency. J. Biol. Chem. *285*, 22244–22253.

Mannes, A.M., Seiler, A., Bosello, V., Maiorino, M., and Conrad, M. (2011). Cysteine mutant of mammalian GPx4 rescues cell death induced by disruption of the wild-type selenoenzyme. FASEB J. *25*, 2135–2144.

Maser, R.L., Magenheimer, B.S., and Calvet, J.P. (1994). Mouse plasma glutathione peroxidase. cDNA sequence analysis and renal proximal tubular expression and secretion. J. Biol. Chem. *269*, 27066–27073.

Pader, I., Sengupta, R., Cebula, M., Xu, J., Lundberg, J.O., Holmgren, A., Johansson, K., and Arnér, E.S. (2014). Thioredoxin-related protein of 14 kDa is an efficient L-cystine reductase and S-denitrosylase. Proc. Natl. Acad. Sci. USA *111*, 6964–6969.

Paez, J.G., Jänne, P.A., Lee, J.C., Tracy, S., Greulich, H., Gabriel, S., Herman, P., Kaye, F.J., Lindeman, N., Boggon, T.J., et al. (2004). EGFR mutations in lung cancer: correlation with clinical response to gefitinib therapy. Science *304*, 1497–1500.

Pao, W., Miller, V., Zakowski, M., Doherty, J., Politi, K., Sarkaria, I., Singh, B., Heelan, R., Rusch, V., Fulton, L., et al. (2004). EGF receptor gene mutations are common in lung cancers from "never smokers" and are associated with sensitivity of tumors to gefitinib and erlotinib. Proc. Natl. Acad. Sci. USA *101*, 13306–13311.

Parmenter, T.J., Kleinschmidt, M., Kinross, K.M., Bond, S.T., Li, J., Kaadige, M.R., Rao, A., Sheppard, K.E., Hugo, W., Pupo, G.M., et al. (2014). Response

of BRAF-mutant melanoma to BRAF inhibition is mediated by a network of transcriptional regulators of glycolysis. Cancer Discov. *4*, 423–433.

Pines, G., Köstler, W.J., and Yarden, Y. (2010). Oncogenic mutant forms of EGFR: lessons in signal transduction and targets for cancer therapy. FEBS Lett. *584*, 2699–2706.

Possik, P.A., Müller, J., Gerlach, C., Kenski, J.C.N., Huang, X., Shahrabi, A., Krijgsman, O., Song, J.-Y., Smit, M.A., Gerritsen, B., et al. (2014). Parallel in vivo and in vitro melanoma RNAi dropout screens reveal synthetic lethality between hypoxia and DNA damage response inhibition. Cell Rep. *9*, 1375–1386.

Scholl, C., Fröhling, S., Dunn, I.F., Schinzel, A.C., Barbie, D.A., Kim, S.Y., Silver, S.J., Tamayo, P., Wadlow, R.C., Ramaswamy, S., et al. (2009). Synthetic lethal interaction between oncogenic KRAS dependency and STK33 suppression in human cancer cells. Cell *137*, 821–834.

Scott, L., Lamb, J., Smith, S., and Wheatley, D.N. (2000). Single amino acid (arginine) deprivation: rapid and selective death of cultured transformed and malignant cells. Br. J. Cancer *83*, 800–810.

Son, J., Lyssiotis, C.A., Ying, H., Wang, X., Hua, S., Ligorio, M., Perera, R.M., Ferrone, C.R., Mullarky, E., Shyh-Chang, N., et al. (2013). Glutamine supports pancreatic cancer growth through a KRAS-regulated metabolic pathway. Nature *496*, 101–105.

Stewart, E.L., Tan, S.Z., Liu, G., and Tsao, M.S. (2015). Known and putative mechanisms of resistance to EGFR targeted therapies in NSCLC patients with EGFR mutations-a review. Transl. Lung Cancer Res. *4*, 67–81.

Takac, I., Schröder, K., Zhang, L., Lardy, B., Anilkumar, N., Lambeth, J.D., Shah, A.M., Morel, F., and Brandes, R.P. (2011). The E-loop is involved in hydrogen peroxide formation by the NADPH oxidase Nox4. J. Biol. Chem. *286*, 13304–13313.

Tallal, L., Tan, C., Oettgen, H., Wollner, N., McCarthy, M., Helson, L., Burchenal, J., Karnofsky, D., and Murphy, M.L. (1970). E. coli L-asparaginase in the treatment of leukemia and solid tumors in 131 children. Cancer *25*, 306–320.

Wong-Ekkabut, J., Xu, Z., Triampo, W., Tang, I.M., Tieleman, D.P., and Monticelli, L. (2007). Effect of lipid peroxidation on the properties of lipid bilayers: a molecular dynamics study. Biophys. J. *93*, 4225–4236.

Yagoda, N., von Rechenberg, M., Zaganjor, E., Bauer, A.J., Yang, W.S., Fridman, D.J., Wolpaw, A.J., Smukste, I., Peltier, J.M., Boniface, J.J., et al. (2007). RAS-RAF-MEK-dependent oxidative cell death involving voltage-dependent anion channels. Nature *447*, 864–868.

Yang, W.S., and Stockwell, B.R. (2008). Synthetic lethal screening identifies compounds activating iron-dependent, nonapoptotic cell death in oncogenic-RAS-harboring cancer cells. Chem. Biol. *15*, 234–245.

Yang, W.S., and Stockwell, B.R. (2016). Ferroptosis: death by lipid peroxidation. Trends Cell Biol. *26*, 165–176.

Yang, W.S., SriRamaratnam, R., Welsch, M.E., Shimada, K., Skouta, R., Viswanathan, V.S., Cheah, J.H., Clemons, P.A., Shamji, A.F., Clish, C.B., et al. (2014). Regulation of ferroptotic cancer cell death by GPX4. Cell *156*, 317–331.